ACS OMEGA

Open Access

http://pubs.acs.org/journal/acsodf

Article

Graphite Sheet-Assisted Laser Desorption Ionization-Mass Spectrometry for Small Organic Compound Analysis

Zhuofei Liu, Keishiro Arima, Naomi Nishiki, Ryou Kuwabara, Shinji Ishitani, Toshiro Matsui,* and Mitsuru Tanaka*

Cite This: *ACS Omega* 2024, 9, 27739−27747

Read Online

ACCESS | Metrics & More | Article Recommendations | Supporting Information

ABSTRACT: Carbon-based nanopowders have been used as ionization materials for laser desorption ionization-mass spectrometry (LDI-MS) and are very efficient at detection in low m/z regions. In this study, we aimed to develop a new sheet-type graphite material that possessed a randomly grooved nanostructured surface consisting of developed sp^2-conjugated atomic carbon to facilitate the desorption/ionization of small compounds in LDI-MS. The graphite sheet exhibited higher UV absorption and provided higher ionization efficiency and survival yield in the LDI-MS detection of a thermometer ion, 4-chloro-benzopyridinium, than those of highly oriented graphite plates. These properties demonstrate that the present graphite sheet is suited for use as an LDI-MS material. Graphite sheet-assisted LDI-MS successfully detected various substances, including amino acids, peptides, and polyethylene glycol polymers, with higher ion intensities and less noise than those associated with conventional organic matrix-assisted LDI-MS (MALDI-MS). Furthermore, graphite sheet-assisted LDI-MS analysis provided more peaks (252 peaks) derived from soy sauce than those obtained by MALDI-MS (36 peaks) and required fewer preparation processes (dilution and air-dried) compared with previously established graphite carbon black-assisted LDI-MS (171 peaks) in the positive mode. This study demonstrates that graphite sheet-assisted LDI-MS has the potential for small organic compound analyses in the biomedical and food science fields.

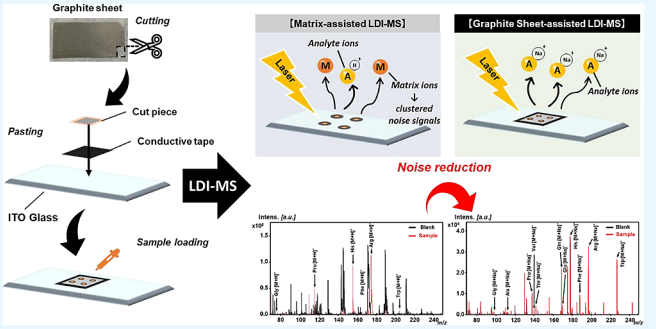

INTRODUCTION

Recently, surface-assisted laser desorption ionization-mass spectrometry (SALDI-MS), a soft ionization technology, has attracted increasing attention in fields such as food safety,[1,2] medical diagnosis,[3,4] and environmental evaluation.[5] Compared with matrix-assisted laser desorption ionization-mass spectrometry (MALDI-MS), which uses organic materials such as α-cyano-4-hydroxycinnamic acid (CHCA), 2,5-dihydroxybenzoic acid (DHB), and *trans*-3-indole acrylic acid (IAA) as a matrix, SALDI-MS uses nanomaterials on the surface of a target-plate to assist energy transfer during the desorption/ionization process of analytes. Therefore, unlike the MALDI spectrum, which contains a large amount of background interference generated by matrix clusters in the low-mass region (m/z < 400), SALDI-MS detects small molecules because of its low noise and high sensitivity. To assist in transferring the light energy received by the surface to the analyte, the surface nanomaterial for SALDI should have excellent photoabsorption properties. Currently, nanostructured substrates consisting of gold[6,7] and silver nanoparticles,[8] titania,[9] silica,[10,11] and carbon-based nanomaterials[12] effectively increase the laser desorption ionization (LDI) efficiency of analytes.

Among the materials used for LDI-MS, carbon has a series of allotropes (e.g., graphite,[13,14] graphene,[15−17] graphdiyne,[18] carbon nanotubes,[19,20] and fullerene[21]) that exhibit high thermal and electrical conductivities, low heat capacities, and excellent UV absorption abilities. These characteristics are strongly related to the efficiency of the LDI process and ensure that carbon-based nanomaterials are often used as surface substrates for SALDI-MS. Graphite, in particular, one of the most promising materials, has been designed (colloidal graphite) to detect low-molecular-weight compounds, such as lanthanides and their oxides[22] and polyethylene glycols.[23]

In our previous study, we successfully accomplished the simultaneous detection of taste- and odor-active compounds using graphite carbon black (GCB)[24] and demonstrated that graphite-assisted SALDI-MS can be utilized in small-molecule analyses and measured in positive and negative modes

Received: May 13, 2024
Revised: May 28, 2024
Accepted: June 7, 2024
Published: June 14, 2024

https://doi.org/10.1021/acsomega.4c04524
ACS Omega 2024, 9, 27739−27747

Scheme 1. Schematic Diagram of Manufacturing Processes of Graphite Sheet

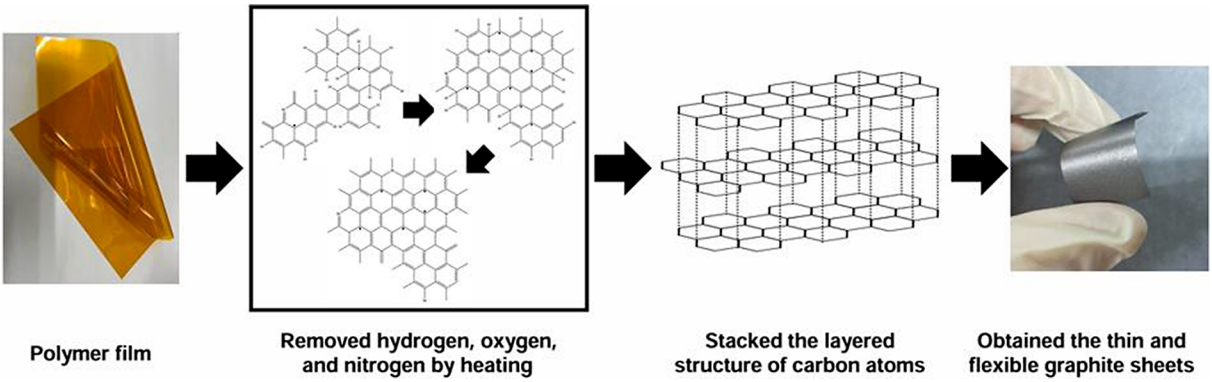

simultaneously compared with using a conventional organic matrix. Furthermore, graphite comprises stacked multilayer graphene which contains π-bonds on the two-dimensional plane to absorb UV laser energy.[25,26] Thus, graphite can be processed into thin sheets as the surface material for SALDI, which improves the reproducibility of the results and allows for the potential application to imaging analysis. The advantages are attributed to the sheet structure, which can prevent inhomogeneous distribution caused by the aggregation of carbon particles; additionally, the ductility of the graphite sheets ensures convenience and flexibility during operation (Scheme 1). Moreover, unlike powdered graphite materials, graphite sheets have a lower risk of machine malfunction in LDI-MS ion sources, owing to the crystal plane of graphite spreading. Thus, sheet-type flexible carbon materials providing good reproducibility and reducing such machine issues are required for efficient LDI-MS detection.

In this study, we aimed to develop a new graphite sheet with flexible and thin characteristics as a highly convenient and useful SALDI material. The new graphite sheet showed better capability associated with LDI efficiency than the graphite plate. The graphite sheet-assisted LDI-MS was able to analyze small molecules such as peptides and amino acids, which are common compounds present in biological and food samples. In addition, the present study included a real food sample analysis using graphite sheet-assisted LDI-MS, suggesting that the new graphite sheet has great advantages for assisting LDI-MS.

EXPERIMENTAL SECTION

Chemicals and Materials. α-Cyano-4-hydroxycinnamic acid (CHCA), angiotensin I (Ang I), angiotensin II (Ang II), polyethylene glycol (PEG) 300, and PEG 1000 were obtained from Sigma-Aldrich (Merck, Darmstadt, Germany). Glycine (Gly), serine (Ser), proline (Pro), valine (Val), cysteine (Cys), leucine (Leu), asparagine (Asn), aspartic acid (Asp), glutamine (Gln), glutamic acid (Glu), histidine (His), phenylalanine (Phe), arginine (Arg), tryptophan (Trp), and D-glucose were obtained from Nacalai Tesque, Inc. (Kyoto, Japan). Alanine (Ala), threonine (Thr), methionine (Met), and *trans*-3-IAA were purchased from FUJIFILM Wako Pure Chemical Co. (Osaka, Japan). PEG 1500 was purchased from Katayama Chemical Industries Co. Ltd. (Osaka, Japan). Glycyl-sarcosine (Gly-Sar) was purchased from Bachem AG (Bubendorf, Switzerland), and Gly-Sar-Sar-Sar-Sar was purchased from Biomatik (Wilmington, DE, USA). [$^{13}C_6$]Glucose and [$^{13}C_5$, $^{15}N_1$]glutamate were obtained from Cambridge Isotope Laboratories, Inc. (Tewksbury, MA, USA). The 1-(4-chlorobenzyl) pyridinium chloride (4-C-BP) salt powder was obtained from Tokyo Chemical Industry Co., Ltd. (Tokyo, Japan). The Japanese soy sauce (dark) was purchased from a local supermarket. All of the reagents mentioned above were used without further purification.

Characterization of Structure and Morphology of Graphite Sheets. A scanning electron microscopy (SEM) image of a graphite sheet was acquired using a field-emission scanning electron microscope, Hitachi HR-SEM SU8000 (HITACHI High Tech. Co., Saitama, Japan), at an accelerating voltage of 1.5 kV; a SEM image of a graphite plate was acquired using a field-emission scanning electron microscope, Hitachi HR-SEM SU3500 (HITACHI High Tech. Co., Saitama, Japan), at an accelerating voltage of 15.0 kV. Raman spectra were recorded in the range of 800−3500 cm^{-1} using a LabRAM ARAMIS spectrometer (Horiba, Kyoto, Japan). The UV−vis spectra were collected using a UV−vis-NIR spectrophotometer, SolidSpec-3700DUV (Shimadzu, Kyoto, Japan).

Preparation of Graphite Sheets and Graphite Plate. Hydrogen, oxygen, and nitrogen were removed from a polyimide film by firing at 1000 °C for 1 h in an oxygen-free state. Thereafter, the remaining carbon atoms were recrystallized by heating to form a layered structure at 3000 °C, in which hexagonal network crystals of carbon atoms were stacked. The graphite sheet was pressed at 2 MPa/cm^2. The obtained graphite sheets, which were flexible and thin, were used in subsequent experiments.

For the production process of graphite plates, the native graphite was crushed into fine particles and mixed with the binder (e.g., resin, clay). After that, the mixture was pressed and heated, which could remove impurities from the binder and became harder. Finally, a thick graphite plate could be obtained and used in subsequent experiments.

Laser Desorption Ionization-Mass Spectrometry Analysis of Small Molecules. The graphite sheets were immersed in MS-grade ethanol (Merck, Darmstadt, Germany) and gently shaken for one min to clean the surface. The graphite sheet was then removed from ethanol and air-dried for 20 min to completely evaporate the ethanol from the surface. A conductive aluminum foil double-sided tape (Teraoka Seisakusho, Tokyo, Japan) was attached to an indium tin oxide (ITO)-coated glass slide (Bruker Daltonics, Bremen, Germany) to fix the graphite sheet onto the glass slide.

To evaluate the ionization profile of the graphite sheet-assisted LDI-MS, amino acid analysis was performed according

https://doi.org/10.1021/acsomega.4c04524
ACS Omega 2024, 9, 27739−27747

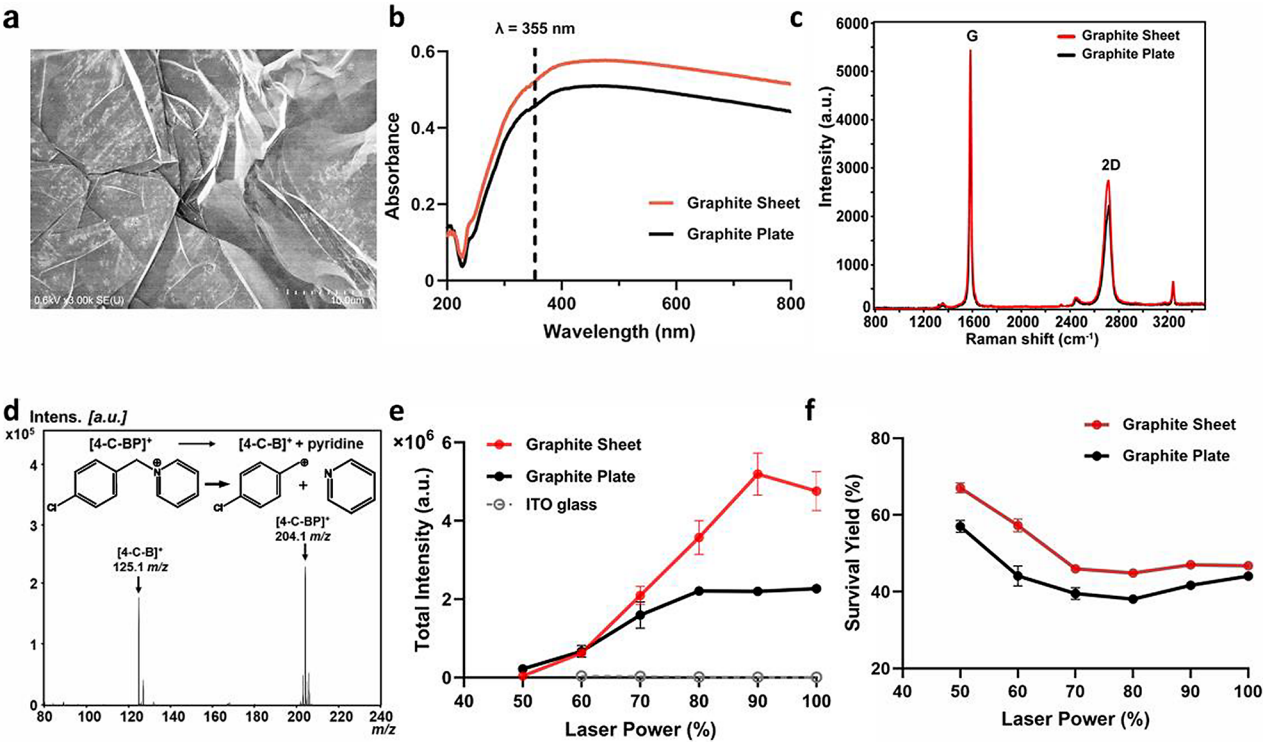

Figure 1. Characterization and ionization profiles of graphite sheet in laser desorption ionization-mass spectrometry. (a) SEM images of the graphite sheets were acquired using a field-emission scanning electron microscope, Hitachi HR-SEM SU8000 at an accelerating voltage of 1.5 kV; the inserted scale bar is 10 μm. (b) UV−vis spectra (200−800 nm) of the graphite sheet (red line) and plate (black line) were obtained using a UV−vis-NIR spectrophotometer, SolidSpec-3700DUV. (c) Raman spectra of graphite sheet (red line) and graphite plate (black line) were recorded in the range of 800−3500 cm^{-1} using a LabRAM ARAMIS spectrometer. (d) Mass spectrum of 4-C-BP was obtained using graphite sheet-assisted laser desorption ionization-mass spectrometry. (e) Total intensity and (f) survival yield values of the 4-C-BP molecule detected by LDI-MS using the graphite sheet (red line), graphite plate (black line), and ITO glass (gray line) were calculated according to the equations described in the Experimental Section.

to our previous report.[24] From among the standard 20 amino acids, 12 amino acids were chosen for analyses using the positive mode, including Gly, Ala, Pro, Val, Thr, Cys, Gln, Glu, His, Phe, Arg, and Trp; and 17 amino acids, Gly, Ala, Ser, Pro, Val, Thr, Cys, Leu, Asn, Asp, Gln, Glu, Met, His, Phe, Arg, and Trp, were prepared for negative mode analyses. The m/z values of the Na^+ adducts of Cys, Leu, Asp, Glu, Met, and Phe overlapped with those of the K^+ adducts of Ser, Pro, Val, Leu, Asp, and Met, respectively, in the positive mode, and Leu, Ile, Gln, and Lys had the same molecular weight. All amino acids were dissolved in MS-grade water (Merck) to prepare 10 mmol/L stock solutions. Gly-Sar, Gly-Sar-Sar-Sar-Sar, Ang I, and Ang II were dissolved in MS-grade water to prepare 1 mmol/L stock solutions. PEG 300, PEG 1000, PEG 1500, and PEG 10,000 were dissolved in MS-grade water to prepare 1 mmol/L stock solutions. Soy sauce was diluted 10−10,000 times with MS-grade water, and the optimized conditions for soy sauce were selected for further analyses. For the quantitative analysis of soy sauce, [$^{13}C_6$]glucose and [$^{13}C_5$, $^{15}N_1$]glutamate were used as internal standards, and different concentrations of glucose were added to the diluted sample solution.

For MALDI-MS, the amino acid solution and diluted soy sauce solution were mixed with an equal volume of matrix solution (CHCA for positive and IAA for negative, each at 10 mg/mL in 70% acetonitrile), and the 0.5 μL sample solution was spotted (1 mmol/L, each at 500 pmol/0.5 μL spot) onto an ITO-coated glass slide and air-dried.

For graphite sheet-LDI-MS, a 0.5 μL amino acid solution was spotted (1 mM, each at 500 pmol/0.5 μL spot) onto a graphite sheet and air-dried. The peptides of Gly-Sar, Gly-Sar-Sar-Sar-Sar, Ang I, and Ang II were spotted (1 mM, each at 500 pmol/0.5 μL of spherical peptides) onto the graphite sheet and air-dried. PEG 300, PEG 1000, PEG 1500, and PEG 10,000 were spotted (1 mM, each at 500 pmol/0.5 μL spot) onto a graphite sheet and air-dried. Soy sauce solution with different dilution factors (10−10,000-fold) was spotted (each at 0.5 μL spot) onto a graphite sheet and air-dried. Because of the hydrophobic surface of graphite sheets, the spots of different aqueous sample solutions could deposit on the surface of the graphite sheets as a droplet.

Evaluation of Ion-Desorption Efficiency and Internal Energy Transfer. Benzylpyridinium (BP) ions have been successfully applied as thermometer probes to determine the internal energy transfer on the surface and evaluate the ion-desorption efficiency in SALDI-MS.[27] The total intensity (TI) of the BP ions was calculated using eq 1 to evaluate the efficiency of the LDI process, where I_M and I_F represent the intensities of the parent ions of 4-C-BP ([M^+] = 204.0 m/z) and the fragment ions of 4-C-B^+ ([F^+] = 125.0 m/z), respectively.

$$TI = I_M + I_F \quad (1)$$

By calculating the survival yield (SY) using eq 2, the extent of internal energy transfer on the surface of the different substrates could be clarified.

https://doi.org/10.1021/acsomega.4c04524
ACS Omega 2024, 9, 27739−27747

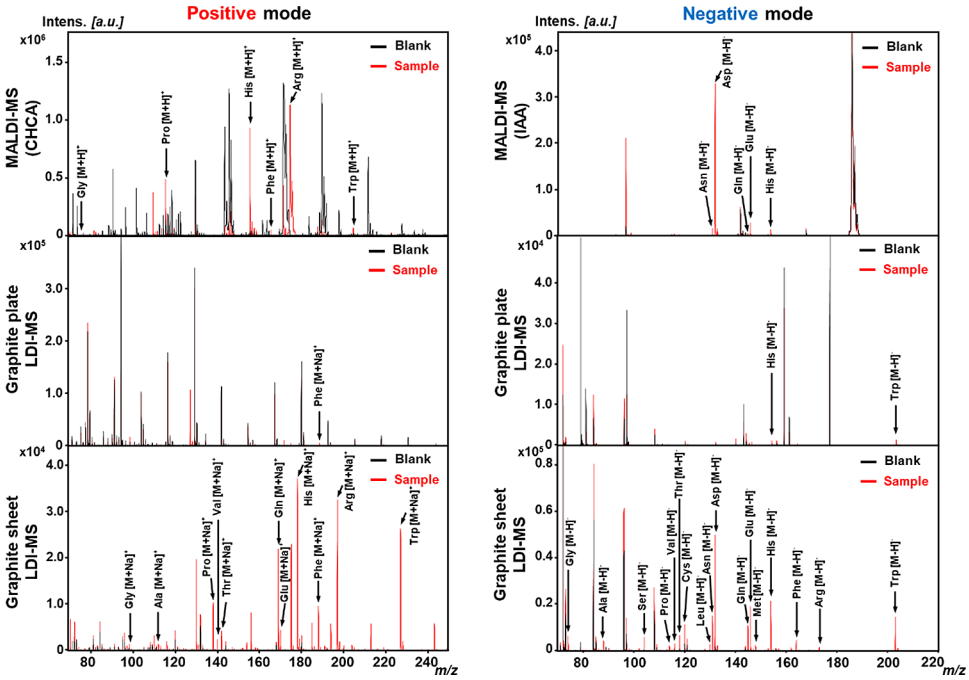

Figure 2. Amino acid analyses were performed by MALDI-MS, graphite plate-assisted laser desorption ionization-mass spectrometry, and graphite sheet-assisted laser desorption ionization-mass spectrometry. MS spectra of a mixture of amino acids were obtained using MALDI-MS, graphite plate-assisted LDI-MS, and graphite sheet-assisted LDI-MS. Positive and negative MALDI-MS spectra were acquired using CHCA and IAA (10 mg/mL each) as matrix reagents, respectively. The matrix solution was mixed with an equal volume of the amino acid mixture, and an aliquot (0.5 μL) of the mixture was spotted onto an ITO-coated glass slide (each at 500 pmol/0.5 μL). MS spectra from graphite plate-assisted LDI-MS and graphite sheet-assisted LDI-MS in positive and negative modes were obtained by measuring the amino acid mixture solution (each at 500 pmol/0.5 μL spot) spotted on each surface. Overlay spectra of the blank (black line) and sample (red line) are shown for MALDI-MS, graphite plate-assisted LDI-MS, and graphite sheet-assisted LDI-MS analyses. The LDI-MS measurement conditions are described in the Experimental Section.

$$\mathrm{SY} = \frac{I_M}{I_M + I_F} \quad (2)$$

4-C-BP was dissolved in MS-grade methanol (Kanto Chemical, Tokyo, Japan) to obtain a 20 mmol/L standard solution. A 0.5 μL aliquot of the 4-C-BP solution was spotted (each at 500 pmol/0.5 μL of spot in 50% MeOH) onto a graphite sheet, graphite plate, and ITO glass. After being air-dried, the target plates were subjected to LDI analysis.

Surface-Assisted Laser Desorption Ionization-Mass Spectrometry Analysis. The sample spots were measured using an AutoFlex III with smart beam II (Nd:YAG 355 nm, Bruker Daltonics) in positive and negative modes. A total of 169 pixels with a raster width of 100 μm were set as the region of analysis to incorporate the sample spot. The detection mass range of the MS data was 0−2000 m/z. Detailed MS parameters were as follows: ion source 1, 20.00 kV; ion source 2, 18.80 kV; lens voltage, 7.50 kV; detector gain, 10.5; laser offset, 59%; laser value, 6.0%; laser power, 60% (positive ion mode), 55% (negative ion mode); laser frequency, 200 Hz; and shot, 100 shots/pixel. The MS spectra were analyzed using Bruker flexAnalysis 3.3 software.

RESULTS AND DISCUSSION

Characterization of Graphite Sheets as an Ionization Material for Laser Desorption Ionization-Mass Spectrometry. Graphite and its various allotropes[24,28] are excellent materials for use in LDI-MS. In this study, a graphite sheet was produced, as depicted in Scheme 1. A graphite plate comprising a highly oriented graphene structure was used as the reference SALDI material, which showed a different appearance with graphite sheets (Figure S1). The morphology of the graphite sheet was observed using SEM (Figure 1a); the images illustrate that the graphite sheet comprised overlapping folded sheets on a submicrometer scale. Because a micrometer-scale structure is essential to facilitate ionization by laser energy transfer,[29] the surface roughness of the graphite sheet enhances the LDI process. On the contrary, there was no rough structure found in the SEM image of the graphite plate, only the flat surface (Figure S2). The UV spectrum shows the absorption of the graphite sheet and graphite plate in the range of 200−800 nm. Both the graphite sheet and graphite plate exhibited comparably high UV absorption at an LDI-laser wavelength of 355 nm (ABS > 0.45) compared to that of the graphene oxide that was used as a SALDI surface.[30] Moreover, the graphite sheet exhibited a higher absorption capacity at an LDI-laser wavelength of 355 nm in comparison to that of the graphite plate (Figure 1b); the higher absorption capacity ensures efficient energy transfer to the analytes. Two major peaks were observed in the Raman spectrum (Figure 1c) at 1582 and 2717 cm^{-1}, corresponding to the G and 2D bands,[31] respectively. The G band, which is a characteristic peak of graphite, is related to the sp^2 hybridization structure.[32] The 2D band corresponds to the charge density of the intrinsic graphene.[33] Therefore, the graphite sheet displayed a profile in the Raman spectrum similar to that of a graphite plate with a complete graphene structure.

To evaluate the desorption/ionization efficiency and internal energy transfer of the graphite sheet during the LDI process, 4-C-BP chloride salt was used as a chemical thermometer. As shown in Figure 1e,f, the present SALDI-MS method showed good reproducibility because much fewer preparation

https://doi.org/10.1021/acsomega.4c04524
ACS Omega 2024, 9, 27739−27747

procedures avoided the additional impact. In addition, since graphite plates possess extremely uniform surface structures, small variations of the obtained peak intensity were observed. When the internal energy of $[4\text{-C-BP}]^+$ (M^+) increases over the critical point of the dissociation reaction, 4-C-BP ions, which contain a C−N bond, are cleaved to form fragments of $[4\text{-C-B}]^+$, (F^+), and pyridine (Figure 1d). The ion-desorption and energy transfer efficiencies of the graphite sheet, graphite plate, and ITO glass were determined based on the SY and TI values. Compared with ITO glass, which could not detect BP ions, a higher TI value was obtained using graphite plate-assisted LDI-MS (Figure 1e), indicating that the graphite plate exhibits significant ionization power when used as the SALDI plate, owing to its excellent energy conversion.[34] The TI of the graphite sheet was markedly higher than that of the graphite plate (Figure 1e). The TI value of the graphite sheet continued to increase as the laser power increased to 90%, and the maximum TI value measured using the graphite sheet was 2.36-fold higher than that of the graphite plate at a laser power of 90% (Figure S3). Moreover, the SY value of the graphite sheet was higher than those of the graphite plate and ITO glass at laser powers of 50−100% (Figure 1f). In general, higher TI values are caused by higher laser energy absorption on the surface, resulting in a lower SY value due to the acceleration of fragmentation.[35] Yang et al.[29] reported that the nanostructured surface facilitated efficient energy transfer to the analytes; therefore, it may be postulated that the microscale folded sheet structure of the graphite sheet might contribute to efficient ionization in LDI-MS. The graphite sheet which displayed high TI and SY values was more suited to the analysis of small compounds; thus, more intact target analyte ions survived and were detected, along with less fragmentation in the LDI process at a specific laser power.

Amino Acid Analysis and Ionization Mechanism of Graphite Sheet-Assisted Laser Desorption Ionization-Mass Spectrometry. To explore the feasibility of using the graphite sheet in the analysis of small molecules, amino acids were subjected to LDI-MS analysis using a conventional matrix, graphite plate, and graphite sheet. Using MALDI-MS, only 6 and 5 amino acids were detected in the positive and negative modes, respectively, because of the significant background interference in the low m/z region. The graphite plate could ionize only Phe in the positive mode; in the negative mode, only His and Trp could be detected with low intensity (Figure 2).

Regarding the graphite sheet, fewer background signals derived from carbon-clustered ions with Δ12 m/z difference were observed than that in the graphite plate, which allows detection of small organic compounds. In fact, as shown in Figure 2, 12 amino acids were successfully detected in the positive mode mainly as $[M + Na]^+$ in the present experimental condition, except for Cys, because of the overlapping noise signals, using graphite sheet-assisted LDI-MS. Since the source of Na^+ may be expected to derive from the experimental condition, such as solvent, glass plate, machine, and so forth, it should be noted that the ratio of possible ion adduct formation (e.g., $[M + H]^+$, $[M + Na]^+$, $[M + K]^+$) may fluctuate depending on the experimental condition. Moreover, all 17 amino acids were detected successfully using graphite sheet-assisted LDI-MS in the negative mode. These results demonstrate that the graphite sheet is useful for SALDI-MS in both positive and negative modes. The intensity could be considered as the ion yield, which is related to the ionization/desorption efficiency. The thermochemical quantities, such as the proton affinity or gas-phase acidity of analytes, could influence the ionization efficiency in LDI-MS.[36] Thus, to investigate the ionization mechanism of graphite sheet-assisted LDI-MS, correlation plots were obtained, in which the intensities of the sum of the observed adduct ions, $[M + H]^+$, $[M + Na]^+$, and $[M + K]^+$, for the amino acids were linearly correlated with the proton affinity (R = 0.911, Figure 3a, correlation plots for each ion

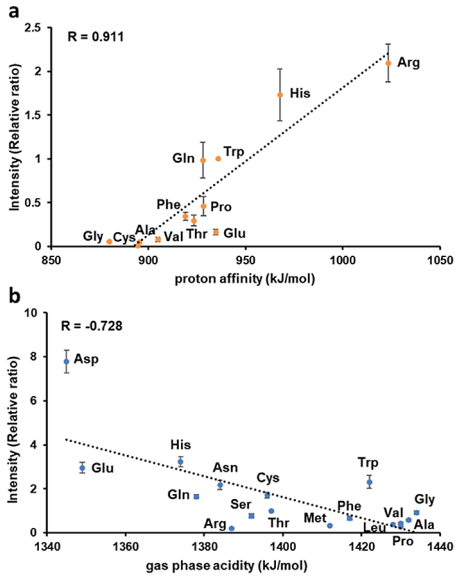

Figure 3. Correlation plots of relative intensities of amino acids obtained by graphite sheet-assisted laser desorption ionization-mass spectrometry (sum intensity of $[M + H]^+$, $[M + Na]^+$, $[M + K]^+$ for positive mode and $[M - H]^-$ for negative mode) to their (a) proton affinity and (b) gas-phase acidity for positive and negative modes, respectively.

adduct are shown in Figure S4); the negative intensities of the $[M-H]^-$ ions were correlated with the gas-phase acidity (R = −0.728, Figure 3b). Meanwhile, the observed correlation strength between intensity and proton affinity in the positive mode was consistent with that between proton affinity and sodium ion affinity of amino acids reported by Kish et al.[37]

Notably, Arg, which has a strong proton affinity, produces a significant yield of $[M + H]^+$ ions (175.3 m/z), which induces a lower intensity of the $[M + Na]^+$ ion in the positive mode (Figure S4). In addition, the acidic nature of Asp might be the reason for the higher intensity of its peak compared with those of the other amino acids in the negative mode. Despite their small difference of gas-phase acidity, Asp showed significantly higher intensity than Glu. A similar trend has also been observed in previous studies using our previous GCB-LDI-MS[24] and other SALDI-MS using TiO_2 nanoparticles,[38] which clearly supports that such a small difference in specifically higher acidic nature could provide higher ionization efficiency of Asp compared with Glu.[39] Conversely, Arg with much higher basicity than His and Cys, which is related to the protonation reaction, suppressed the ion yield of Arg $[M - H]^-$.[39] The ionization mechanism of graphite sheet-assisted LDI-MS displayed a linear correlation between the proton affinities of amino acids and the positive ion intensities of $[M + Na]^+$ and between the gas-phase acidity and the ion intensities

https://doi.org/10.1021/acsomega.4c04524
ACS Omega 2024, 9, 27739−27747

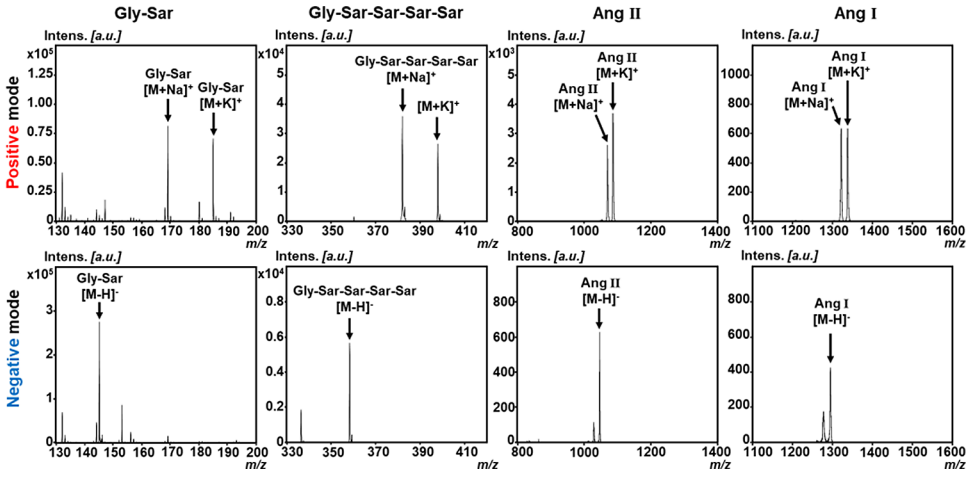

Figure 4. Mass spectra of small peptides (Gly-Sar, Gly-Sar-Sar-Sar-Sar, Ang I, and Ang II) using graphite sheet-assisted laser desorption ionization-mass spectrometry. MS spectra of the small peptides were obtained using graphite sheet-assisted LDI-MS in positive and negative modes. The peptides of Gly-Sar, Gly-Sar-Sar-Sar-Sar, Ang I, and Ang II were spotted (each at 500 pmol/0.5 μL spot) onto the graphite sheet. The LDI-MS measurement conditions are described in the Experimental Section.

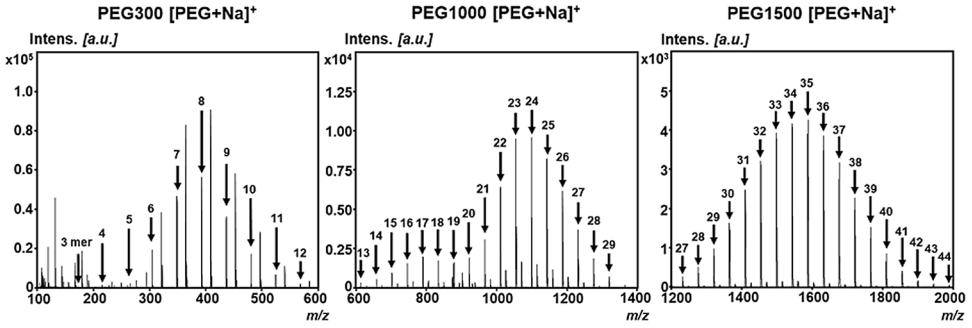

Figure 5. Mass spectra of PEG (MW 300−1500) using graphite sheet-assisted laser desorption ionization-mass spectrometry. MS spectra of the PEGs were obtained by using graphite sheet-assisted LDI-MS in the positive mode. PEG 300, PEG 1000, and PEG 1500 were spotted (each at 500 pmol/0.5 μL spot) onto the graphite sheet. The peaks of $[PEG + Na]^+$ were labeled in the mass spectrum as the form of 3−44 mer. The LDI-MS measurement conditions are described in the Experimental Section.

in the negative mode, similar to our previously reported GCB-LDI-MS.[24]

Detectable Mass Detection Range of Graphite Sheet-Assisted Laser Desorption Ionization-Mass Spectrometry. To evaluate the detectable molecular size by graphite sheet-assisted LDI-MS, peptides (e.g., Gly-Sar, Gly-Sar-Sar-Sar-Sar, Ang I, and Ang II) and synthetic polymers (e.g., PEGs) were used. All peptides were successfully detected in the positive mode (Figure 4), and the main peaks were the sodium and potassium adducts of the analytes.

By contrast, in the negative mode, Gly-Sar $[M - H]^-$, Gly-Sar-Sar-Sar-Sar $[M - H]^-$, Ang II $[M - H]^-$, and Ang I $[M - H]^-$ were clearly detected at 145.2, 358.9, 1045.2, and 1295.5 m/z, respectively using graphite sheet-assisted LDI-MS (Figure 4). Thus, although the detected intensities of peptides decreased with increasing peptide length, the graphite sheet-assisted LDI-MS method has the advantage of peptide analysis up to ∼1000 Da in both positive and negative modes. Furthermore, PEGs with different average molecular weights (300, 1000, and 1500 m/z) were used to define the mass detection range of graphite sheet-assisted LDI-MS. A series of PEG peaks were observed in the mass range of 100−2000 m/z in the mass spectrum as $[M + Na]^+$ (Figure 5); however, no peaks could be observed in the spectrum of PEG 10,000. SALDI-MS methods are usually focused on the analysis in the low-mass region compared with MALDI-MS. For instance, Yang et al.[29] have reported that the stainless-steel surface could detect PEG with 500−1500 Da but not >2000 Da because the surface generated less fragments ions, which meant the suitable desorption and ionization ability for small organic compounds and not for high molecular weight compounds. The above results indicate that graphite sheet-LDI-MS can be used to analyze organic compounds with molecular weights <2000 Da in both positive and negative modes.

Application of Graphite Sheet-Assisted Laser Desorption Ionization-Mass Spectrometry for Food Analysis (Soy Sauce). To evaluate the practicality of using the graphite sheet, various metabolites in a fermented food product, soy sauce, were analyzed using graphite sheet-assisted LDI-MS. The soy sauce was directly diluted 10−10,000 times with MS-grade water, and the compounds were analyzed in both positive and negative modes. When the dilution factor of the soy sauce was increased 1000-fold in the positive mode and 100-fold in the negative mode, more signals of higher intensity were observed (Figure S5); therefore, using soy sauce, after 1000 times dilution and 100 times dilution, was the optimal condition for analysis in positive and negative modes, respectively. Peaks at 209.1 m/z in the positive mode and 152.2 m/z in the negative mode, corresponding to $[M + Na]^+$ of $[^{13}C_6]$glucose and $[M - H]^-$ of $[^{13}C_5, {}^{15}N_1]$glutamate

https://doi.org/10.1021/acsomega.4c04524
ACS Omega 2024, 9, 27739−27747

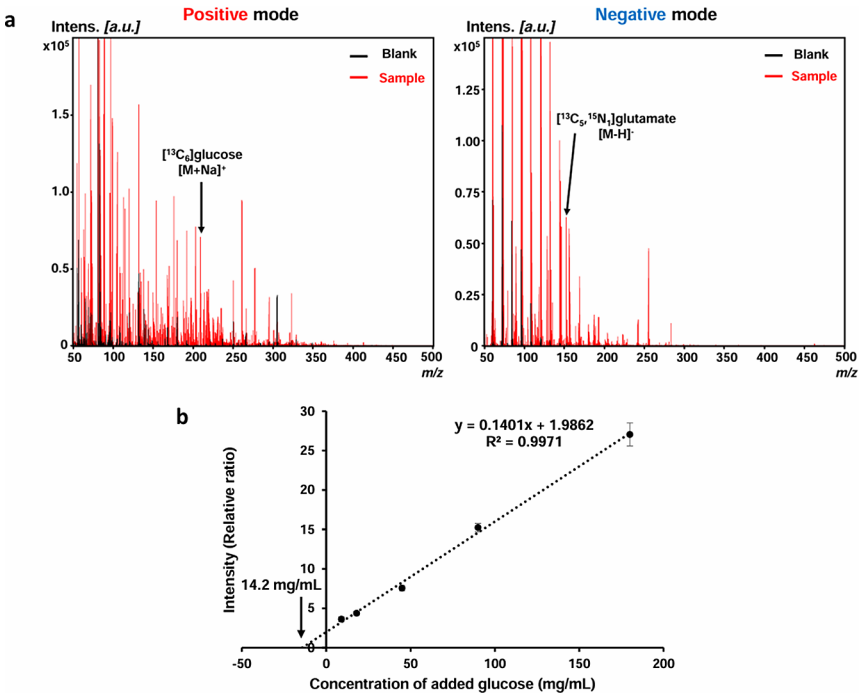

Figure 6. Soy sauce analyses using graphite sheet-assisted laser desorption ionization-mass spectrometry. (a) MS spectra of blank (black line) and metabolites obtained from soy sauce (red line) using graphite sheet-assisted LDI-MS in positive and negative modes by the measurement of 1000-fold, 100-fold diluted soy sauce (0.5 μL) spotted on a graphite sheet attached to an ITO-coated glass slide, respectively. The peaks of internal standards [$^{13}C_6$]glucose and [$^{13}C_5$, $^{15}N_1$]glutamate were obtained using graphite sheet-assisted LDI-MS in positive mode and negative mode, respectively. (b) Standard addition curve was obtained by adding glucose (9−180 mg/mL) spiked with IS (18 mg/mL) to soy sauce. Relative intensity was calculated as the ratio of monosaccharide $[M + Na]^+$ and [$^{13}C_6$]glucose $[M + Na]^+$. The LDI-MS measurement conditions are described in the Experimental Section.

added as internal standards, respectively, were successfully detected (Figure 6a). Compared with conventional MALDI-MS and our previously developed graphite carbon black-assisted LDI-MS,[24] graphite sheet-assisted LDI-MS produced the largest number of peaks from soy sauce (in positive mode: MALDI-MS 36 peaks, GCB-LDI-MS 171 peaks, and graphite sheet-assisted LDI-MS 252 peaks; in negative mode: MALDI-MS 22 peaks, GCB-LDI-MS 259 peaks, and graphite sheet-assisted LDI-MS 289 peaks) (Figure S6). Graphite sheet-assisted LDI-MS also successfully detected peaks corresponding to lactate (113.0 m/z) and monosaccharides (203.1 m/z) in the positive mode, and pyroglutamate (128.2 m/z) and glutamate (146.2 m/z) in the negative mode (Figure S7) in Japanese dark soy sauce, which were also detected by our developed GCB-LDI-MS and identified by the conventional HPLC method in our previous study.[40]

Moreover, to evaluate the linear dose−response and quantitative capability of the graphite sheet-assisted LDI-MS analysis, a concentration series (9−180 mg/mL) of glucose were spiked into the soy sauce to quantify the originally contained glucose by the standard addition method (Figure 6b). These results demonstrate that graphite sheet-assisted LDI-MS shows a linear correlation between the concentration of spiked glucose and the intensity ratio of glucose to IS (R^2 = 0.9971). The quantified glucose level was calculated as 14.2 mg/mL, which is the same level as the reported monosaccharide concentration in Japanese soy sauce (dark) measured by the conventional phenyl-hydrazine-derivatized HPLC method (14.1 mg/mL).[40] Moreover, just like the analysis results of soy sauce, graphite sheet-assisted LDI-MS is also applicable to biological samples, such as plasma, urine, and milk (data not shown).

CONCLUSIONS

We demonstrated that graphite sheet-assisted LDI-MS performs well in small-molecule analysis and practical food applications in both positive and negative modes. The unique surface structure of the graphite sheet contributes to strong UV absorption for the desired energy transfer efficiency, good electrical conductivity, and high sensitivity of the target analytes in LDI-MS. The ionization mechanism of graphite sheet-assisted LDI-MS is similar to that of other carbon materials (e.g., GCB-LDI-MS). In addition, the graphite sheet could be used in food quality analysis, such as that for soy sauce, in which hundreds of MS peaks were detected in both positive and negative modes, and the originally contained glucose was successfully quantified by graphite sheet-assisted LDI-MS. Therefore, the graphite sheets developed in this study are promising SALDI-MS materials that can be used to analyze various target compounds in various scientific fields. On the other hand, although graphite sheet-assisted LDI-MS showed less noise background and higher sensitivity of analytes in the low-mass region than using powder-type carbon materials, it is difficult for the graphite sheet-assisted LDI-MS to detect higher molecular weight compounds (e.g., PEG 10,000), which is a limitation for wider detection of sheet-type material-assisted LDI-MS. Powder-type materials usually have higher UV absorption and energy transfer ability,[41] and nanopowders showed the similar way to combine with the target analytes like MALDI-MS, which may easily improve the efficiency of the LDI process. Based on the mechanism of graphite sheet

https://doi.org/10.1021/acsomega.4c04524
ACS Omega 2024, 9, 27739−27747

assisting LDI process, rougher surface of graphite sheets should contribute to the high LDI efficiency but that may cause the graphite sheets to "peel off" during the manufacturing process because of its structure made of stacked multilayer graphene. Limited by current manufacturing technology, graphite sheets may be further optimized and improved in the future. Moreover, compared with nanopowder materials, sheet-type graphite has the advantage of handling and using easily enough for anyone to acquire the data conveniently, except the time for waiting for the air drying of sample solution spots and also has a lower risk of mechanical problems owing to the dispersal of powdered-type materials. In this case, the present simple and rapid graphite sheet-assisted LDI-MS method has a great potential for widespread general applications in biomedical and food science fields.

■ ASSOCIATED CONTENT

Supporting Information

The Supporting Information is available free of charge at https://pubs.acs.org/doi/10.1021/acsomega.4c04524.

Appearance of graphite sheet and graphite plate; SEM image of graphite plate; MS spectra of 4-C-BP by using graphite sheet-assisted LDI-MS, graphite plate-assisted LDI-MS, and ITO-assisted LDI-MS at 90% laser power; correlation plots of relative intensities of amino acids obtained by graphite sheet-assisted laser desorption ionization-mass spectrometry to their proton affinity; MS spectra of metabolites in soy sauce with different dilution times (10−10,000 times) by using graphite sheet-assisted LDI-MS in positive and negative modes; MS spectra of metabolites in soy sauce (100 times diluted) by using MALDI-MS and GCB-LDI-MS; and MS spectra of metabolites in soy sauce by using graphite sheet-assisted LDI-MS in positive and negative modes (PDF)

■ AUTHOR INFORMATION

Corresponding Authors

Toshiro Matsui − *Faculty of Agriculture, Graduate School of Kyushu University, Fukuoka 819-0395, Japan; Research and Development Center for Five-Sense Devices, Kyushu University, Fukuoka 819-0395, Japan;* orcid.org/0000-0002-9137-8417; Email: tmatsui@agr.kyushu-u.ac.jp

Mitsuru Tanaka − *Faculty of Agriculture, Graduate School of Kyushu University, Fukuoka 819-0395, Japan; Research and Development Center for Five-Sense Devices, Kyushu University, Fukuoka 819-0395, Japan;* orcid.org/0000-0002-8242-5058; Email: mitsurut@agr.kyushu-u.ac.jp

Authors

Zhuofei Liu − *Faculty of Agriculture, Graduate School of Kyushu University, Fukuoka 819-0395, Japan*

Keishiro Arima − *Faculty of Agriculture, Graduate School of Kyushu University, Fukuoka 819-0395, Japan*

Naomi Nishiki − *Manufacturing Innovation Division, Panasonic Holdings Co., Osaka 571-8502, Japan*

Ryou Kuwabara − *Manufacturing Innovation Division, Panasonic Holdings Co., Osaka 571-8502, Japan*

Shinji Ishitani − *Manufacturing Innovation Division, Panasonic Holdings Co., Osaka 571-8502, Japan*

Complete contact information is available at: https://pubs.acs.org/10.1021/acsomega.4c04524

Author Contributions

Z.L., K.A., N.N., T.M., and M.T. designed the experiments. Z.L., K.A., and M.T. performed the experiments. Z.L., K.A., and M.T. analyzed the obtained data, and all authors discussed the results. Z.L. drafted the manuscript. N.N., R.K., S.I., T.M., and M.T. supervised the manuscript. All the authors contributed meaningful feedback for the project and manuscript.

Notes

The authors declare no competing financial interest.

■ ACKNOWLEDGMENTS

This work was partially supported by the JSPS KAKENHI [Grant Numbers JP21H05828 (M.T.), JP21H03798 (M.T.), JP23H04356 (M.T.), and JP21K19089 (T.M.)]. This research was also partially supported by AMED under Grant Number 23ym0126816j0002 and 24ym0126811j0003, and the Center for Clinical and Translational Research of Kyushu University. The authors thank the Center of Advanced Instrumental Analysis, Kyushu University, for technical support during scanning electron microscopy imaging and Raman analysis. This work was partly supported by the "Advanced Research Infrastructure for Materials and Nanotechnology in Japan (ARIM)" of the Ministry of Education, Culture, Sports, Science, and Technology (MEXT). Proposal Number: JPMXP1223KU1004.

■ REFERENCES

(1) López de Laorden, C.; Beloqui, A.; Yate, L.; Calvo, J.; Puigivila, M.; Llop, J.; Reichardt, N.-C. Nanostructured Indium Tin Oxide Slides for Small-Molecule Profiling and Imaging Mass Spectrometry of Metabolites by Surface-Assisted Laser Desorption Ionization MS. *Anal. Chem.* **2015**, *87* (1), 431−440, DOI: 10.1021/ac5025864.

(2) Lai, H.-Z.; Wang, S.-G.; Wu, C.-Y.; Chen, Y.-C. Detection of Staphylococcus Aureus by Functional Gold Nanoparticle-Based Affinity Surface-Assisted Laser Desorption/Ionization Mass Spectrometry. *Anal. Chem.* **2015**, *87* (4), 2114−2120.

(3) Pan, X.-Y.; Chen, C.-H.; Chang, Y.-H.; Wang, D.-Y.; Lee, Y.-C.; Liou, C.-C.; Wang, Y.-X.; Hu, C.-C.; Kuo, T.-R. Osteoporosis Risk Assessment Using Multilayered Gold-Nanoparticle Thin Film via SALDI-MS Measurement. *Anal. Bioanal. Chem.* **2019**, *411* (13), 2793−2802.

(4) Su, Y.; Lai, X.; Guo, K.; Wang, X.; Chen, S.; Liang, K.; Pu, K.; Wang, Y.; Hu, J.; Wei, X.; Chen, Y.; Wang, H.; Lin, W.; Ni, W.; Lin, Y.; Zhu, J.; Ng, K.-M. Covalent Bonding and Coulomb Repulsion-Guided AuNP Array: A Tunable and Reusable Substrate for Metabolomic Characterization of Lung Cancer Patient Sera. *Anal. Chem.* **2022**, *94* (48), 16910−16918.

(5) Kawasaki, H.; Nakai, K.; Arakawa, R.; Athanassiou, E. K.; Grass, R. N.; Stark, W. J. Functionalized Graphene-Coated Cobalt Nanoparticles for Highly Efficient Surface-Assisted Laser Desorption/Ionization Mass Spectrometry Analysis. *Anal. Chem.* **2012**, *84* (21), 9268−9275.

(6) Wang, Y.; Zhang, K.; Tian, T.; Shan, W.; Qiao, L.; Liu, B. Self-Assembled Au Nanoparticle Arrays for Precise Metabolic Assay of Cerebrospinal Fluid. *ACS Appl. Mater. Interfaces* **2021**, *13* (4), 4886−4893.

(7) Qu, X.; Wang, T.; Liu, X.; Jiang, X.; Liang, X.; Wu, J. Dual-Mechanism-Driven Strategy for High-Coverage Detection of Serum Lipids on a Novel SALDI-MS Target. *Anal. Chem.* **2022**, *94* (24), 8570−8579.

(8) Paulson, A. E.; Premasiri, W. R.; Ziegler, L. D.; Lee, Y. J. Use of Nanoparticle Decorated Surface-Enhanced Raman Scattering Active Sol−Gel Substrates for SALDI-MS Analysis. *J. Am. Soc. Mass Spectrom.* **2023**, *34* (2), 273−278.

(9) Kim, M.-J.; Park, J.-M.; Noh, J.-Y.; Yun, T. G.; Kang, M.-J.; Ku, N. S.; Lee, E. H.; Park, K. H.; Park, M. S.; Lee, S.-G; Pyun, J.-C. Coffee Ring Effect Free TiO2 Nanotube Array for Quantitative Laser Desorption/Ionization Mass Spectrometry. *ACS Appl. Nano Mater.* **2020**, *3* (9), 9249−9259.
(10) Wang, X.; Teng, F.; Wang, Y.; Lu, N. Rapid Liquid-Phase Microextraction of Analytes from Complex Samples on Superwetting Porous Silicon for Onsite SALDI-MS Analysis. *Talanta* **2019**, *198*, 63−70.
(11) Zhu, Q.; Wang, Z.; Wang, Y.; Teng, F.; Du, J.; Dou, S.; Lu, N. Investigation of Surface Morphology on Ion Desorption in SALDI-MS on Tailored Silicon Nanopillar Arrays. *J. Phys. Chem. C* **2020**, *124* (4), 2450−2457.
(12) Khajavinia, A.; El-Aneed, A. Carbon-Based Nanoparticles and Their Surface-Modified Counterparts as MALDI Matrices. *Anal. Chem.* **2023**, *95* (1), 100−114.
(13) Kawasaki, H.; Takahashi, N.; Fujimori, H.; Okumura, K.; Watanabe, T.; Matsumura, C.; Takemine, S.; Nakano, T.; Arakawa, R. Functionalized Pyrolytic Highly Oriented Graphite Polymer Film for Surface-Assisted Laser Desorption/Ionization Mass Spectrometry in Environmental Analysis. *Rapid Commun. Mass Spectrom.* **2009**, *23* (20), 3323−3332.
(14) Zhang, J.; Li, Z.; Zhang, C.; Feng, B.; Zhou, Z.; Bai, Y.; Liu, H. Graphite-Coated Paper as Substrate for High Sensitivity Analysis in Ambient Surface-Assisted Laser Desorption/Ionization Mass Spectrometry. *Anal. Chem.* **2012**, *84* (7), 3296−3301.
(15) Zhao, H.; Li, Y.; Wang, J.; Cheng, M.; Zhao, Z.; Zhang, H.; Wang, C.; Wang, J.; Qiao, Y.; Wang, J. Dual-Ion-Mode MALDI MS Detection of Small Molecules with the O−P,N-Doped Carbon/Graphene Matrix. *ACS Appl. Mater. Interfaces* **2018**, *10* (43), 37732−37742.
(16) Juang, Y.-M.; Chien, H.-J.; Chen, C.-J.; Lai, C.-C. Graphene Flakes Enhance the Detection of TiO_2-Enriched Catechins by SALDI-MS after Microwave-Assisted Enrichment. *Talanta* **2016**, *153*, 347−352.
(17) Tang, L. A. L.; Wang, J.; Loh, K. P. Graphene-Based SELDI Probe with Ultrahigh Extraction and Sensitivity for DNA Oligomer. *J. Am. Chem. Soc.* **2010**, *132* (32), 10976−10977.
(18) Luo, P.; Wang, L.; Jiang, L.; Sun, J.; Li, Y.; Liu, H.; Xiong, C.; Nie, Z. Application of Graphdiyne in Surface-Assisted Laser Desorption Ionization Mass Spectrometry. *ACS Appl. Mater. Interfaces* **2021**, *13* (1), 1914−1920.
(19) Bian, J.; Olesik, S. V. Surface-Assisted Laser Desorption/Ionization Time-of-Flight Mass Spectrometry of Small Drug Molecules and High Molecular Weight Synthetic/Biological Polymers Using Electrospun Composite Nanofibers. *Analyst* **2017**, *142* (7), 1125−1132.
(20) Kim, Y.-K.; Min, D.-H. Fabrication of Alternating Multilayer Films of Graphene Oxide and Carbon Nanotube and Its Application in Mechanistic Study of Laser Desorption/Ionization of Small Molecules. *ACS Appl. Mater. Interfaces* **2012**, *4* (4), 2088−2095.
(21) Santos, V. G.; Fasciotti, M.; Pudenzi, M. A.; Klitzke, C. F.; Nascimento, H. L.; Pereira, R. C. L.; Bastos, W. L.; Eberlin, M. N. Fullerenes in Asphaltenes and Other Carbonaceous Materials: Natural Constituents or Laser Artifacts. *Analyst* **2016**, *141* (9), 2767−2773.
(22) Conway, U.; Warren, A. D.; Gates, P. J. A Study of the Application of Graphite MALDI to the Analysis of Lanthanides and Deconvolution of the Isobaric Species Observed. *Analyst* **2021**, *146* (19), 5988−5994.
(23) Conway, U.; Warren, A. D.; Arthur, C. J.; Gates, P. J. A Study of the Application of Graphite MALDI to the Analysis of Short-Chain Polyethylene Glycols. *Polym. Chem.* **2021**, *12* (3), 439−448.
(24) Tanaka, M.; Arima, K.; Takeshita, T.; Kunitake, Y.; Ohno, N.; Imamura, M.; Matsui, T. Laser Desorption Ionization−Mass Spectrometry with Graphite Carbon Black Nanoparticles for Simultaneous Detection of Taste- and Odor-Active Compounds. *ACS Appl. Nano Mater.* **2022**, *5* (2), 2187−2194.
(25) Zheng, X.; Zhang, J.; Wei, H.; Chen, H.; Tian, Y.; Zhang, J. Determination of Dopamine in Cerebrospinal Fluid by MALDI-TOF Mass Spectrometry with a Functionalized Graphene Oxide Matrix. *Anal. Lett.* **2016**, *49* (12), 1847−1861.
(26) Hidayah, N. M. S.; Liu, W.-W.; Lai, C.-W.; Noriman, N. Z.; Khe, C.-S.; Hashim, U.; Lee, H. C. Comparison on Graphite, Graphene Oxide and Reduced Graphene Oxide: Synthesis and Characterization. *AIP Conf. Proc.* **2017**, *1892* (1), 150002.
(27) Liu, X.; Chen, Z.; Wang, T.; Jiang, X.; Qu, X.; Duan, W.; Xi, F.; He, Z.; Wu, J. Tissue Imprinting on 2D Nanoflakes-Capped Silicon Nanowires for Lipidomic Mass Spectrometry Imaging and Cancer Diagnosis. *ACS Nano* **2022**, *16* (4), 6916−6928.
(28) Hinners, P.; Lee, Y. J. Carbon-Based Fingerprint Powder as a One-Step Development and Matrix Application for High-Resolution Mass Spectrometry Imaging of Latent Fingerprints. *J. Forensic Sci.* **2019**, *64* (4), 1048−1056.
(29) Yang, J.; Zhang, W.; Zhang, H.; Zhong, M.; Cao, W.; Li, Z.; Huang, X.; Nie, Z.; Liu, J.; Li, P.; Ma, X.; Ouyang, Z. Polydopamine-Modified Substrates for High-Sensitivity Laser Desorption Ionization Mass Spectrometry Imaging. *ACS Appl. Mater. Interfaces* **2019**, *11* (49), 46140−46148.
(30) Kim, Y.-K.; Min, D.-H. Mechanistic Study of Laser Desorption/Ionization of Small Molecules on Graphene Oxide Multilayer Films. *Langmuir* **2014**, *30* (42), 12675−12683.
(31) Zhao, H.; Li, Y.; Zhao, H.; Zhao, Z.; Wang, J.; Zhang, R. Yolk-Shell Ni/NiO Anchored on N-Doped Graphene Synthesized as Dual-Ion MALDI Matrix for Detecting and Imaging Bioactive Small Molecules. *J. Colloid Interface Sci.* **2022**, *613*, 285−296.
(32) Pardo, H.; Divine Khan, N.; Faccio, R.; Araújo-Moreira, F. M.; Fernández-Werner, L.; Makarova, T.; Mombrú, Á. W. Raman Characterization of Bulk Ferromagnetic Nanostructured Graphite. *Physica B Condens. Matter* **2012**, *407* (16), 3206−3209.
(33) Frank, O.; Mohr, M.; Maultzsch, J.; Thomsen, C.; Riaz, I.; Jalil, R.; Novoselov, K. S.; Tsoukleri, G.; Parthenios, J.; Papagelis, K.; Kavan, L.; Galiotis, C. Raman 2D-Band Splitting in Graphene: Theory and Experiment. *ACS Nano* **2011**, *5* (3), 2231−2239.
(34) Shi, C. Y.; Deng, C. H. Recent Advances in Inorganic Materials for LDI-MS Analysis of Small Molecules. *Analyst* **2016**, *141* (10), 2816−2826.
(35) Kurczy, M. E.; Zhu, Z.-J.; Ivanisevic, J.; Schuyler, A. M.; Lalwani, K.; Santidrian, A. F.; David, J. M.; Giddabasappa, A.; Roberts, A. J.; Olivos, H. J.; O'Brien, P. J.; Franco, L.; Fields, M. W.; Paris, L. P.; Friedlander, M.; Johnson, C. H.; Epstein, A. A.; Gendelman, H. E.; Wood, M. R.; Felding, B. H.; Patti, G. J.; Spilker, M. E.; Siuzdak, G. Comprehensive Bioimaging with Fluorinated Nanoparticles Using Breathable Liquids. *Nat. Commun.* **2015**, *6* (1), 5998.
(36) Nishikaze, T.; Takayama, M. Study of Factors Governing Negative Molecular Ion Yields of Amino Acid and Peptide in FAB, MALDI and ESI Mass Spectrometry. *Int. J. Mass Spectrom.* **2007**, *268* (1), 47−59.
(37) Kish, M. M.; Ohanessian, G.; Wesdemiotis, C. The Na+ affinities of α-amino acids: side-chain substituent effects. *Int. J. Mass Spectrom.* **2003**, *227*, 509−524.
(38) Yonezawa, T.; Asano, T.; Nguyen, M. T. Desorption and Ionization of Amino Acid Compounds Observed by Negative Ion Mode Surface-Assisted Laser Desorption/Ionization Mass Spectrometry (SALDI-MS) using Titanium Oxide Nanoparticles. *Nano Biomed.* **2020**, *12* (2), 101−109.
(39) Jones, C. M.; Beriner, M.; Carson, E.; Colyer, K.; Metz, R.; Pawlow, A.; Wischow, E.; Webb, I.; Andriole, E.; Poutsma, J. Gas-phase acidities of the 20 protein amino acids. *Int. J. Mass Spectrom.* **2007**, *267*, 54−62.
(40) Tanaka, M.; Arima, K.; Ide, H.; Koshi, M.; Ohno, N.; Imamura, M.; Matsui, T. Application of graphite carbon black assisted-laser desorption ionization-mass spectrometry for soy sauce product discrimination. *Biosci. Biotechnol. Biochem.* **2024**, *88*, 656−664.
(41) Müller, W. H.; Verdin, A.; De Pauw, E.; Malherbe, C.; Eppe, G. Surface-assisted laser desorption/ionization mass spectrometry imaging: A review. *Mass Spec Rev.* **2022**, *41*, 373−420.

https://doi.org/10.1021/acsomega.4c04524
ACS Omega 2024, 9, 27739−27747